CrystEngComm

Accepted Manuscript

ROYAL SOCIETY OF CHEMISTRY

www.rsc.org/crystengcomm

Journal Name

RSCPublishing

ARTICLE

2:1 5-Fluorocytosine-Acesulfame CAB Cocrystal and 1:1 5-Fluorocytosine-Acesulfame Salt Hydrate with Enhanced Stability against Hydration

Cite this: DOI: 10.1039/x0xx00000x

Received 00th January 2012,
Accepted 00th January 2012

DOI: 10.1039/x0xx00000x

www.rsc.org/

Lin Wang,[ac] Xiaonan Wen,[b] Ping Li,[a] Jianming Wang,[b] Ping Yang,[c] Hailu Zhang*[a] and Zongwu Deng*[a]

5-Fluorocytosine (FC), a widely used antifungal drug, has poor physical stability under different relative humidity (RH) condition, which may trigger serious challenges during its drug product development. In this contribution, a conjugate acid–base (CAB) cocrystal and a salt hydrate of FC were obtained with an artificial sweetener, Acesulfame (AH), in molar ratios of 2:1 (FCAH21) and 1:1 (FCAH11), respectively. The result products were characterized by a variety of analytical methods, including single crystal and powder X-ray diffractions (XRD), differential scanning calorimetry (DSC), nuclear magnetic resonance (NMR), as well as dynamic vapor sorption (DVS). ^{13}C and ^{15}N solid state NMR spectra provide solid evidences on the CAB cocrystal/salt formation. At room temperature, moisture sorption data show the new forms are nonhygroscopic/slightly hygroscopic, and resistant to FC hydrate formation at high RH condition (> 80%). FCAH21 has higher FC content and presents more favorable thermal stability than those of FCAH11, which make it more attractive for further pharmaceutical application.

Introduction

Over 80% of active pharmaceutical ingredients (APIs) and their final drug products are developed as solids due to the ease of handling and lower production and storage costs.[1] For a given API compound, it can exist in several different solid forms, such as polymorphs and amorphous of pure API compound, hydrate, solvate, salt, and cocrystal. The different solid forms of an API may further differ significantly in their physicochemical properties, and thereafter the bioavailability, stability and manufacturability of the solid drug.[2–3] Thus, it is crucial to understand the solid form landscape of an API to ensure suitable properties on the one hand. On the other hand, solid forms offer straightforward way to dramatically adjust the physicochemical and biological properties of parent APIs. Pharmacetical salt is most often used form (more than 50%) in the pharmaceutical industry.[4–5] Similar to pharmaceutical salt, cocrystal is another type of multi-component crystalline complex that has attracted wide interest in recent years.[6] The main difference between salt and cocrystal is whether complete proton transfer occurred between API and the guest molecule.[7]

5-Fluorocytosine (FC, Scheme 1) is a synthetic antifungal drug and widely used for the treatment of Candida and Cryptococcus.[8] Also, FC is a potential drug used for cancer treatment.[9] Form I is the thermodynamically most stable phase at room temperature, and has been used in the marketed products.[10] However, the physical stability of this anhydrous form is very poor because a monohydrate can be formed when the drug is exposed to higher relative humidity (RH, > 80%) (Figure 1a).[11a] Moreover, when the RH condition switches from high to low, dehydration occurs (RH < 25%) and a metastable Form II can also be formed along with Form I (Figure 1b). Such complicated phase changes induce serious challenges during the processing and storage of FC.

Pharmaceutical salt or cocrystal formation is a potential way to tackle the moisture stability problem. FC is a basic molecule with acid dissociation constant (pK_a) of 3.26,[12] and various salt forms has been reported with salicylic acid (pK_a = 2.98), saccharin (SAC, Scheme 1, pK_a = 2.2), oxalic acid (pK_a = 1.25), maleic acid (pK_a = 1.91), fumaric acid (pK_a = 3.03), etc.,[11–13] as well as cocrystal forms with 5-nitrouracil (pK_a = 5.66), 2-aminopyrimidine (pK_a = 3.46), etc.[14–16] Three salts, 5-fluorocytosinium chloride/5-fluorocytosine monohydrate ($FC{\cdot}FCH^+Cl^-{\cdot}H_2O$), 1:1 saccharin salt and 2:1 oxalate, were demonstrated as stable forms against RH change though the former exhibits risks of uncontrolled dehydration at elevated temperature.[11,17,18a] The $FC{\cdot}FCH^+Cl^-{\cdot}H_2O$, which contains a hemi-fluorocytosinium ($FC{\cdot}FCH^+$), can also be termed as a hydrate of conjugate acid–base (CAB) cocrystal.[18b] The CAB cocrystals differ from either conventional salt or conventional

cocrystal in which the two cocrystallizing species are chemically related with a difference of only a proton.[18b]

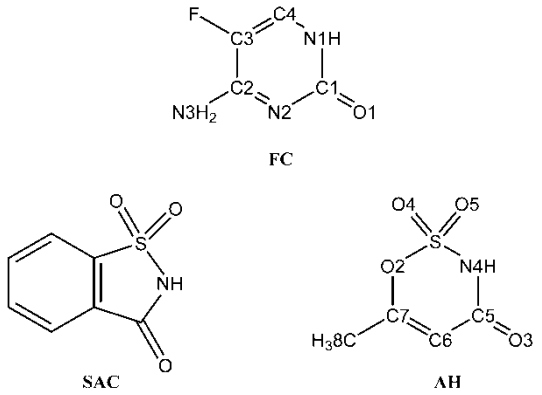

Scheme 1 Molecular structures of 5-fluorocytosine (FC, pK_a = 3.26), saccharin (SAC, pK_a = 2.2) and acesulfame (AH, pK_a = 2.0).

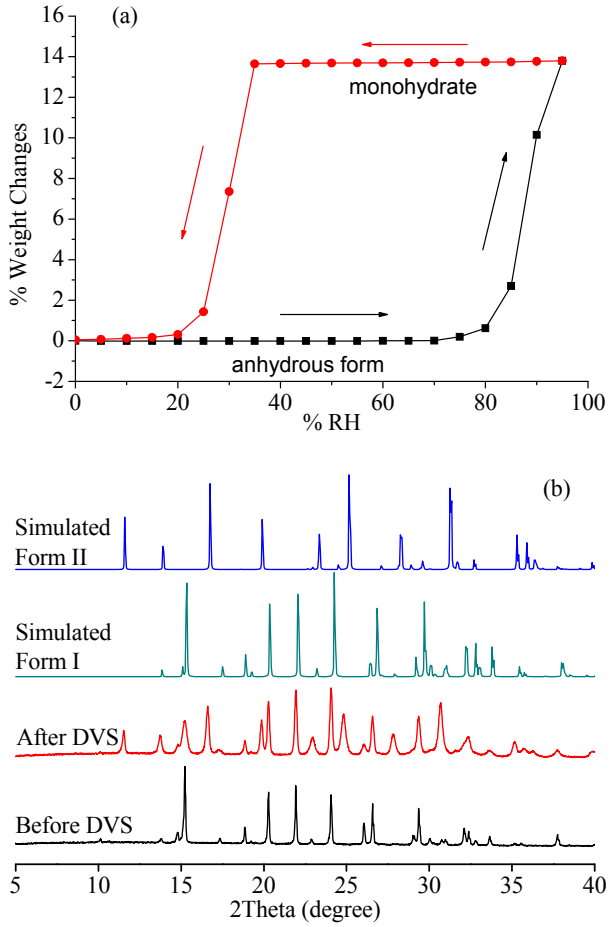

Fig. 1 DVS curve of FC at 25 °C (a); Powder XRD patterns of FC before and after DVS test (b). The simulated powder XRD curves were obtained by using *Mercury 3.3*.

Given an API and a guest molecule, whether they forms as a conventional salt or a conventional cocrystal can be predicted by the pK_a rule.[7,19] When the Δp*K*a (Δp*K*a = p*K*a(base) − p*K*a(acid)) is greater that 3 (or 2, or 3.75), salt is likely to be formed. If Δp*K*a < 0, cocrystal formation is expected. When Δp*K*a is in the range of 0 ~ 3 (or 2, or 3.75), it is difficult to predict the ionization state. CAB cocrystal should follow the rule for conventional salt formation due to the existence of intermolecular proton transfer in such system. For FC, intermolecular proton migration (forming FCH^+ or $FC{\cdot}FCH^+$) would preferentially occur in the continuum range ($0 < \Delta pKa < 3$).[12]

Structural resemblance strategy is often employed for cocrystal/salt design and screening.[20,21] As mentioned above, a 1:1 SAC salt of FC was reported recently with enhanced stability against hydration.[11a] In this contribution, an aliphatic calorie-free sweetener acesulfame (AH, Scheme 1) is selected as guest molecule to prepare salt with FC due to its similar function groups (O=C−N−SO2) and p*K*a value to SAC. However detailed characterization, to identify both the ionization states and physicochemical properties, is required to determine if this will lead to formation of new FC forms.

Experimental

Materials

FC (≥ 98%) and methanol (≥ 99.5%) were purchased from Sinopharm Chemical Reagent Co., Ltd (Shanghai, China). Potassium salt of Acesulfame (AK, ≥ 99.9%) was purchased from Xiya Chemical Reagent Co., Ltd (Chengdu, China). The free acid form of Acesulfame, AH (Scheme 1), was obtained by following the procedure reported by Velaga.[22] Ultrapure water (18.2 MΩ·cm) was used throughout the experiments. Other chemicals used were of analytical grade and used as received without any further purification.

Synthesis of 2:1 5-Fluorocytosine-Acesulfame CAB Cocrystal (FCAH21) by solvent evaporation

FC (25.8 mg, 0.2 mmol) and AH (16.3 mg, 0.1 mmol) were dissolved in 10 mL of water or methanol. The resulting solution was filtered through 0.22 μm PTFE syringe filter and left to slowly evaporate at room temperature. Colorless crystal of FCAH21 was harvested after 1−3 week. Large-scale crystallization of FCAH21 can be realized through water evaporation of the 2:1 aqueous solution at elevated temperature (60−80 °C). In either experimental condition, single-crystal sample of FCAH21 can be easily obtained.

Synthesis of single-crystal 1:1 5-Fluorocytosine-Acesulfame Salt Hemihydrate (FCAH11) by stationary crystallization

FC (64.5 mg, 0.5 mmol) and AH (326.3 mg, 2.0 mmol) were dissolved in 2.5 mL of water at 60 °C, then the resulting solution was filtered through 0.22 μm PTFE syringe filter. The solution was sealed in a glass sample bottle and maintained at room temperature. After several minutes, colorless crystal of FCAH11 can be obtained.

Synthesis of powder FCAH11 by freeze-drying

Equimolar quantities of FC (51.6 mg, 0.4 mmol) and AH (65.2 mg, 0.4 mmol) were dissolved in 10 mL of ultrapure water. The

resulting solution was filtered through 0.22 μm PTFE syringe filter and transferred into plastic centrifuge tubes and rapidly frozen using liquid nitrogen. The plastic centrifuge tubes were then delivered into CoolSafe 55-4 freeze dryer (ScanVac, Lynge, Denmark) equipped with a Vacuubrand RZ-2.5 vacuum pump (Vacuubrand, Wertheim, Germany). Fine powder sample was obtained after 72 h freeze-drying at −60 °C. The stoichiometric ratio (FC:AH = 1:1) of the product was confirmed by using ^{1}H liquid NMR on a Varian 400 MHz spectrometer (Varian, Inc., Palo Alto, CA). The water content of the product (theoretical value: 2.99%; experimental value: ~3.0%) was detected with the Karl-Fischer (KF) titration method on an 870 KF Titrino plus titrator (Metrohm AG, Herisau, Switzerland).

Single-crystal X-ray siffraction (Single-crystal XRD)

Single-crystal XRD measurement was conducted on Bruker APEX-II CCD diffractometer (Bruker AXS, Karlsruhe, Germany) with Mo Kα radiation (λ = 0.71073 Å) at 153 or 240 K. Diffraction data were processed (cell refinement and data reduction) using Bruker SAINT and APEX2 software.[23] The structure was solved by direct methods using SHELXS-97 program and refined against F^2 using SHELXL-97 program.[24] All non-hydrogen atoms were refined with anisotropic displacement parameters, and all hydrogen atoms were positioned with calculated positions and refined with fixed isotropic displacement parameters. Relevant crystal data, collection parameters, and refinement results can be found in Table 1. ORTEP representations of FCAH21 and FCAH11 were provided in Supporting Information (Figure S1&S2).

Powder X-ray diffraction (Powder XRD)

Powder XRD measurements were conducted on PANalytical X'Pert Pro X-ray powder diffractometer (PANalytical B.V., Almelo, Netherlands) equipped with an X'Celerator Real Time Mutil-Strip detector. A Cu Kα radiation was used at 45 kV and 40 mA. Samples were scanned in the reflection mode from 3 to 40° 2θ with a scanning step size of 0.0167° and a counting time per step of 16 s. For FCAH21 and FCAH11, comparisons of the experimental and theoretical powder patterns after Rietveld refinement were given in Supporting Information (Figure S3&S4).

Differential scanning calorimetry (DSC)

DSC data were collected on TA Q2000 differential scanning calorimeter (TA Instruments, New Castle, DE). Approximately 3 mg of sample was hermetically sealed in an aluminum pan and heated from 25 °C with scan rate of 10.0 °C/min under nitrogen atmosphere (50 mL/min). Temperature calibration was performed using NIST traceable indium metal.

Solid state nuclear magnetic resonance (Solid state NMR)

Solid state ^{13}C and ^{15}N cross-polarization magic angle spinning (CP/MAS) spectra were performed with a 4 mm double-resonance MAS probe on a Bruker AVANCE III-500 spectrometer (Bruker BioSpin, Karlsruhe, Germany) operating at a magnetic field strength of 11.7 T. For ^{13}C experiments, a total sideband suppression (TOSS) frame was embedded into the conventional Cross-Polarization (CP) pulse sequence. The Hartmann-Hahn conditions of the CP experiment for acquiring ^{13}C and ^{15}N spectra were optimized by using adamantane and L-glycine, respectively. ^{13}C NMR spectra were obtained at an 8 kHz MAS spinning speed with a 2.0 ms contact time. ^{15}N NMR spectra were obtained at an 8 kHz MAS spinning speed with a 7.0 ms contact time. Recycle delays for FC, AH, FCAH11, and FCAH21 were set at 200 s, 8 s, 8 s, and 8 s, respectively. The ^{13}C and ^{15}N chemical shifts were externally referenced to tetramethylsilane (δ = 0.0 ppm) and L-glycine (δ = −347.0 ppm), respectively.

Table 1 Crystallographic Data for FCAH11 and FCAH21

Name	FCAH11	FCAH21
Formula	$C_{16}H_{20}F_2N_8O_{11}S_2$	$C_{12}H_{13}F_2N_7O_6S$
formula weight	602.52	421.35
T(K)	240.00(10)	153(2)
crystal system	monoclinic	Triclinic
space group	C 1 2/c 1	P-1
a (Å)	26.3596(11)	7.2613(2)
b (Å)	5.8523(3)	10.5289(3)
c (Å)	32.3137(11)	11.6662(4)
α (°)	90.00	66.8180(11)
β (°)	105.987(4)	82.0220(12)
γ (°)	90.00	78.5670(12)
V (Å^3)	4792.0(3)	801.81(4)
Z/Z'	8/2	2/1
$\rho_{calculated}$ (g·cm^{-3})	1.670	1.745
F(000)	2480	432
R_{int}	0.0442	0.0357
reflns collected	25239	26053
unique reflns	4908	3270
observed reflns	3737	2996
number parameters	387	269
absorption coeff (mm^{-1})	0.313	0.278
crystal size (mm)	0.4×0.12×0.1	0.53×0.40×0.18
GOF on F^2	1.010	1.057
$R_1[I > 2\sigma(I)]/R_1$[a]	0.0451/0.0672	0.0305/0.0335
$wR_2[I > 2\sigma(I)]/wR_2$[b]	0.0978/0.1066	0.0840/0.0866
CCDC	992732	978203

[a]$R1 = \| F_o\| - |F_c\| / \sum |F_o|$. [b]$wR_2 = \{[w(F_o^2 - F_c^2)^2]/ w(F_o^2)^2]\}^{1/2}$.

Dynamic vapor sorption (DVS)

Moisture stability tests were conducted on a DVS Intrinsic dynamic gravimetric water sorption analyser (SMS Ltd., London, UK) at 25.0 ± 0.1°C. About 20 mg of samples were placed in the quartz sample pan. The RH was increased from 0% to 95% in sorption process and then decreased from 95% to 0% in desorption process with the step size of 5% RH. The

sample was equilibrated at each step with the equilibration criteria of either dm/dt ≤ 0.0001 or maximum equilibration time of 2 h.[11] For FCAH21 and FCAH11, the first equilibration criteria of each step can be always achieved within 2 h. The solids after DVS tests were subjected to powder XRD measurements to monitor possible solid forms transformation.

Results and discussion

Formation and crystal structure of FCAH21

Both FCH^+ and $FC{\cdot}FCH^+$ states have been observed recently. While, once an organic acidic molecule (salicylic acid, dicarboxylic acids) is used, FCH^+ ion more likely exists in the salt.[12,13] The pursuing of novel FC/AH crystal complex via crystallization was first conducted in aqueous solution with a starting FC:AH ratio of 1:1. In contrary to the FCH^+ salts formed with the other organic molecules in water, a CAB cocrystal ($FC{\cdot}FCH^+{\cdot}AH^-$), FCAH21, can be obtained consistently. Single crystal samples can be also easily obtained under this (starting FC:AH ratio of 1:1, water as solvent) and above mentioned (experimental section) crystallization conditions. The experimental/simulated XRD patterns and crystal structure of FCAH21 are shown in Figure 2 and Figure 3, and comparison of the experimental and theoretical powder patterns after Rietveld refinement was given in Supporting Information (Figure S3). Perumalla *et al.* reported that FC can crystalize with SAC in methanol, resulting to a $FC{\cdot}FCH^+{\cdot}SAC^-$ monomethanol solvate.[11a] While for AH, the solvent molecule can not be incorporated into the unit cell when methanol was used as solvent, and FCAH21 is always obtained.

Single crystal XRD analysis reveals that the FCAH21 crystallizes in the triclinic space group (P-1) with two asymmetric units in a crystal cell (Z=2) which are in inversion relationship (Z'=1). Each asymmetric unit contains one FCH^+ cation, one FC molecule and one AH^- anion as a consequence of a proton transfer from N4 of AH to N2' of FC.

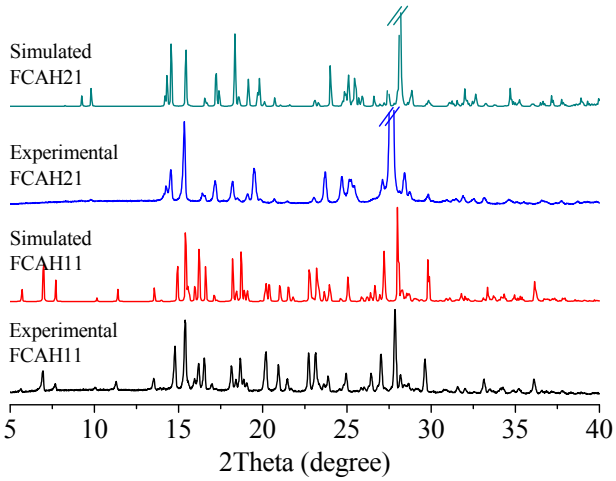

Fig. 2 Experimental and simulated powder XRD patterns of FCAH11 and FCAH21. FCAH11 and FCAH21 were obtained by freeze-drying and solvent (water) evaporation methods, respectively.

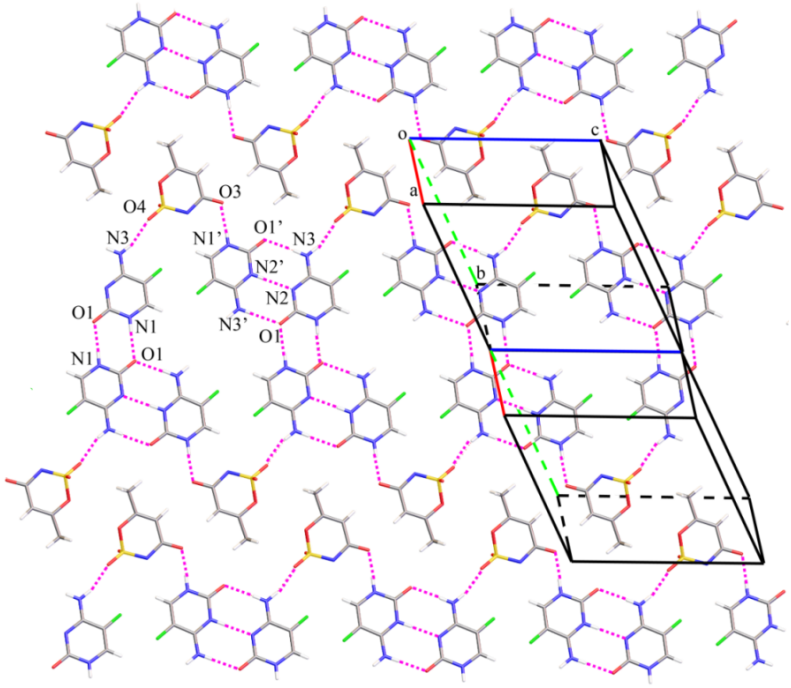

Fig. 3 One sheet of the layered structure of FCAH21. The hydrogen bonds are indicated as dashed lines.

The hydrogen bonds involved in the layered structure are indicated as dashed lines in Figure 3. In one asymmetric unit, AH^- anion interacts with the FCH^+ cation and FC molecule via N1'H···O3 and O4···HN3 hydrogen bonding, respectively. A robust three-point synthon (N3H···O1', N2'H···N2, and N3'H···O1) is observed in the $FC{\cdot}FCH^+$ duplexes fraction.

Such base-pair like interactions have been used in crystal engineering for many years which consistently exist in the CAB cocrystals (previously named hemi-fluorocytosinium salts).[11a,17,18a] For fluorocytosinium salts, two-point synthon is often involved (*vide infra*). Thus, the more stable triple hydrogen bonding structure should be an important contributor to the preferred crystallization of the FC·FCH$^+$ over FCH$^+$ species.[18a] Hydrogen bonds between adjacent asymmetric units in the layer structure are also formed between two FC molecules via a pair of N1H···O1. As a result, a 40-membered ring motif containing two AH$^-$ anions, two FCH$^+$ and four FC molecules is formed (Figure 3). Treating the ring motif as a unit, every two adjacent ring units are connected by hydrogen bonds between FCH$^+$ cations and FC molecules, resulting in a stable 2D sheet structure (Figure 3).

Among the adjacent layers, the FC molecule/AH$^-$ anion/FCH$^+$ cation in FCAH21 is arranged in ABC fashion as shown in Figure 4. In addition, interlayer hydrogen bonds are observed between AH$^-$ anions and FCH$^+$ cations (N3'H···O5). Given the unique hydrogen-bonding interactions in the CAB cocrystal, one may expect some modified physicochemical properties for FCAH21. Especially, the robust three-point synthon between FC and FCH$^+$, as well as interactions between AH$^-$ and FC/FCH$^+$ may block the interaction between FC/FCH$^+$ and physical adsorbed water molecules, and resistant to FC hydrate formation.

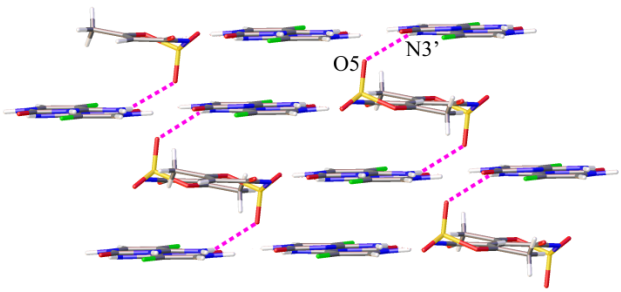

Fig. 4 The hydrogen-bonding interactions between the layers of FCAH21 viewed along c axis. The hydrogen bonds are indicated as dashed lines.

Formation and crystal structure of FCAH11

As FC is a high dose drug,[11b] FCAH21 should be the more promising one due to the higher API content than that of 1:1 FC/AH crystal complex. While for a crystallography investigation, FCAH11 is also expected to be obtained. Fluorocytosinium salt may be formed when excessive H$^+$ is present in the solution.[18a] For the current system, FCAH11 can be obtained when AH is significant excess in the water solution (FC:AH = 1:4). This salt is a hemihydrate and crystallized in a monoclinic space group (C 1 2/c 1) with eight asymmetric units in a crystal cell (Z=8, Z'=2). FC molecules are completely protonated at N2 and N2' sites by accepting protons from AH molecules.

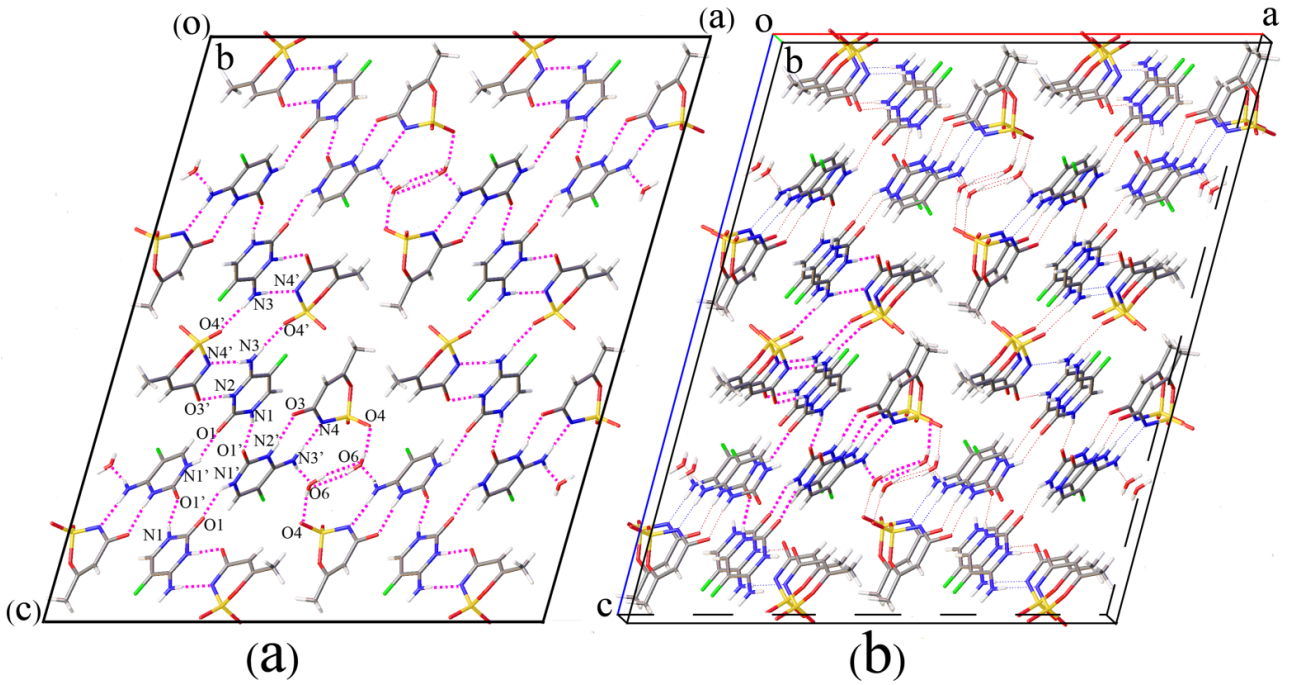

Fig. 5 Crystal packing diagram of FCAH11. 2D view (a) and 3D view (b) along the b axis. One disordered H atom in H_2O is omitted for clarity. The hydrogen bonds are indicated as dashed lines.

Figure 5 shows one crystal cell of FCAH11. The salt mainly adopts two $R_2^2(8)$ heterosynthons, N3H···N4'/N2H···O3' and N3'H···N4/N2'H···O3 hydrogen-bonding pairs, between FCH$^+$ and AH$^-$. Such kind of $R_2^2(8)$ synthon is often observed in the fluorocytosinium salts (1:1 FCH$^+$/saccharin$^-$, 1:1 FCH$^+$/salicylic acid$^-$, 2:1 FCH$^+$/oxalic acid^{2-}, 1:1 FCH$^+$/maleic acid$^-$, and 2:1 FCH$^+$/fumaric acid^{2-}).[11–13] A closed 12-membered ring motif and an unclosed 16-membered "ring motif" are displayed

in Figure 5a, and those relevant hydrogen-bonding interactions are actually formed among molecules at different cross-sections (Figure 5b). Additionally, hydrogen-bonding interactions between water molecule and FCH^+ (O6···HN3'), AH^- (O6H···O4 or O6H···O5), and other water (O6H···O6) are also observed. Similar to FCAH21, modified physicochemical properties are also expected due to the salt formation.

Though the single-crystal sample of FCAH11 was obtained, such nonstoichiometric operation should not be the optimal choice with high yield and physical purity (AH impurity contained, detected by ^{13}C CP/MAS NMR spectrum, not shown here) if it is employed to prepare bulk sample. Recently, Jones *et al.* reported that new polymorphs of pharmaceutical cocrystal can be screened out by using freeze-drying.[25] Given that the FC and AH molecules can be kept homogeneously during the freeze-drying process, we employed this approach to prepare bulk sample of FCAH11 salt with a starting FC:AH ratio of 1:1. As shown in Figure 2, the result product yields a set of distinctive diffraction pattern, which is in line with the simulated pattern derived from the FCAH11 structure, confirming the successfully bulk sample preparation.

^{13}C and ^{15}N solid state NMR

The question of ionization in multi-component crystal systems is often discussed if the crystal structure is not solved. In fact, such issue is also concerned even single-crystal sample is obtained because the light proton atoms are posited via calculation rather than experimental detection during the structure refinement. Nitrogen atom is always involved in the protonation or deprotonation in a salt or a CAB cocrystal,[4,26] thus ^{15}N solid state NMR spectrum may be used to assess the protonation states since complete proton transfer should lead to significant ^{15}N chemical shift change. FC/AH complexes must represent one of the most complicated conditions when we talk about the ionization states for multi-component crystal systems, for both of FC and AH contain activated nitrogen sites, and AH molecule can also exist in enol form (Scheme 2).[27,28]

The ^{13}C CP/MAS TOSS NMR spectra of FC (Form I), AH (Form I), and their complexes are shown in Figure 6. The fingerprint spectra confirm that the number of molecules per asymmetric unit (Z') are equal to 1, 2, 1, and 2 for form I FC, form I AH, FCAH21, and FCAH11, respectively. For example, form I AH exhibits the Z' information by the signal splitting at C8 (19.35 & 20.59 ppm), C5 (165.37 & 165.70 ppm), and C7 (168.18 & 168.52 ppm) sites.

With the formation of FCAH21, the maximum chemical shift changes occurs on C1' (7.23 ppm) of protonated FC and C5 (6.38 ppm) of AH^- anion, respectively. Generally, the repacking of molecules in a different crystal cell often leads to a ^{13}C chemical shift change less than 5 ppm. Thus, the proton transfer between the N sites (N4 of AH anion and N2' of FCH^+) must be a main contributors to these larger ^{13}C chemical shift changes. C3 and C3' give rise to four peaks. Such signal doubling is ascribed to the *J* coupling interaction ($J_{C\text{-}F}$). The ^{13}C CP/MAS TOSS NMR spectrum of FCAH11 is also shown in Figure 6. Similar to FCAH21, much larger chemical shift changes are observed for C5/5' (9.56 ppm) and C1/1' (8.70 ppm) atoms, which give solid evidence on the occurrence of intermolecular proton transfer.

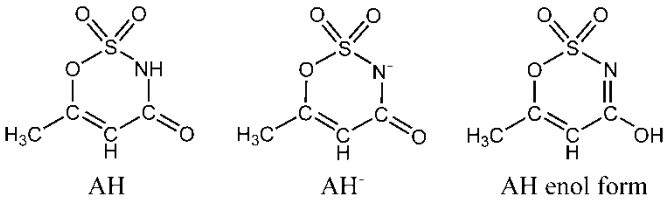

Scheme 2 Molecular structures of AH, AH^- and AH enol form.

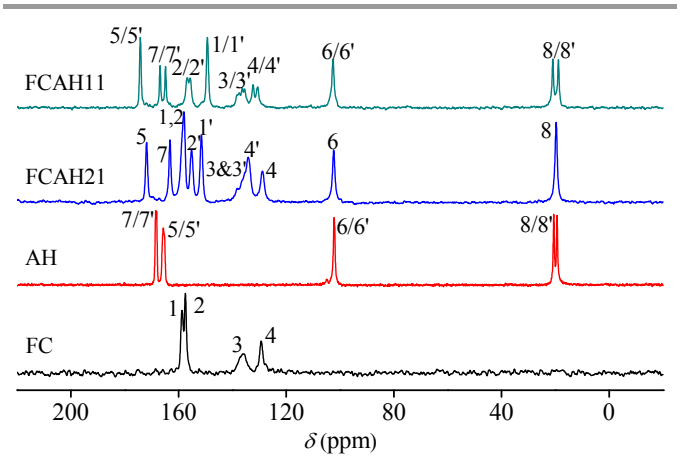

Fig. 6 ^{13}C CP/MAS TOSS NMR spectra of FC (Form I), AH (Form I), FCAH21, and FCAH11.

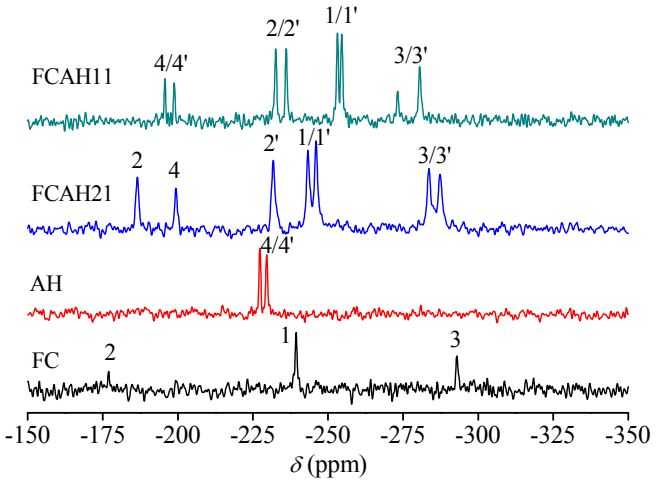

Fig. 7 ^{15}N CP/MAS NMR spectra of FC (Form I), AH (Form I), FCAH21, and FCAH11.

^{15}N CP/MAS NMR spectra of FCAH21 and FCAH11 (Figure 7) provide more information on their ionization states. The formation of FCAH11 salt activates protons transfer from N4 and N4' to bare N2 and N2' sites. Such kind of protonation environment exchanges between NH and bare N must further lead to the ^{15}N chemical shift exchanges relative to the input materials consequently, which can be clearly observed in Figure 7. For FCAH21, only one FC is protonated at N2' site,

then the signals of N2 and N2' appear in different resonance ranges.

Recently, several pharmaceutical crystal complexes of AH have been reported. AH can exist in three states: AH anion, natural AH molecule or enol form molecule (Scheme 2).[22,28,29] For FCAH11, AH may exist in enol form if the proton located between N2(N2') and O3'(O3) is covalently bonded with O3'(O3). For this form, C5(C5') should show a much upfield signal, which can be eliminated according to the ^{13}C spectrum (Figure 6). Also, if AH existed in enol form, then no protons are accepted by N2 and N2' atoms. Thus, a pair of ^{15}N signals of these two nitrogen atoms should appear in the downfield range similar to N2 in the form I FC or FCAH21 sample (Figure 7). All these spectral clues provide valuable inspiration and method towards the judgment of ionization states, especially for the powder crystal samples.

Hygroscopicity and moisture stability

As mentioned in the first section, form I FC exhibits poor physical stability and a monohydrate can be formed when exposed to high RH condition (e,g, RH > 80%). Since both FCAH11 and FCAH21 can be obtained from aqueous solution, they are expected to be stable at high RH condition. As shown in Figure 8, both sample keep their original XRD features after equilibrating at 95% RH for 48 h. Since FCAH11 is a hydrate, its phase stability at low RH condition was also investigated. After equilibrating at 0% RH for 48 h, FCAH11 did not change its solid form (Figure 8), and its water content remained unchanged (~3.0%).

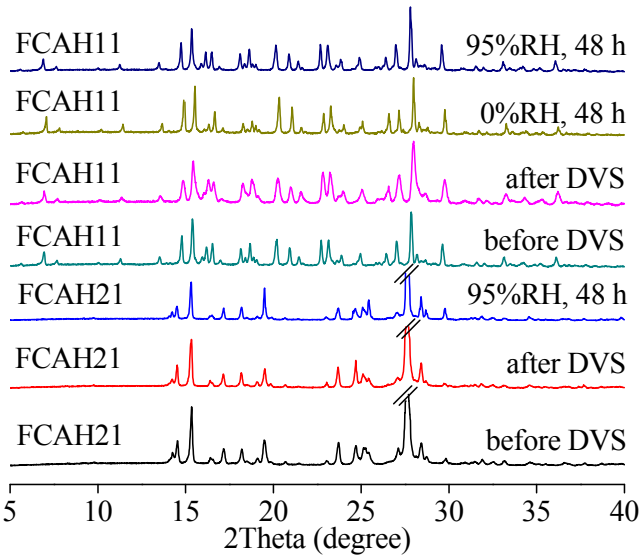

Fig. 8 Powder XRD patterns of FCAH21 and FCAH11 before and after DVS tests and after equilibrating at 0% RH/25 °C or 95% RH/25 °C for 48 h.

DVS tests were also performed for the two novel FC forms and shown in Figure 9. FCAH21 can be regarded as a nonhygroscopic sample because its moisture adsorption is as low as 0.55% (w/w) even at 95% RH. FCAH11 is slightly hygroscopic with water uptakes of 1.22% and 3.84% at 80% and 95% RH, respectively, due likely to that freeze-dried FCAH11 appears as very fine powder sample. Recently, Sun[30] reported that CAB cocrystals exhibit lower hygroscopicity over their corresponding salts, which may due to their reducing of interactions with absorbed water. For FCAH21, more potential hydrogen bonding sites are occupied by intra-crystal hydrogen bonding interactions than that of FCAH11, which may be another contributor to the lower hygroscopicity of FCAH21 than FCAH11. Additionally, both FCAH11 and FCAH21 keep their original XRD features after the moisture sorption/desorption cycle (Figure 8). All these results indicate FCAH11 and FCAH21 have superior phase stability against RH varying and satisfied hygroscopicity at room temperature.

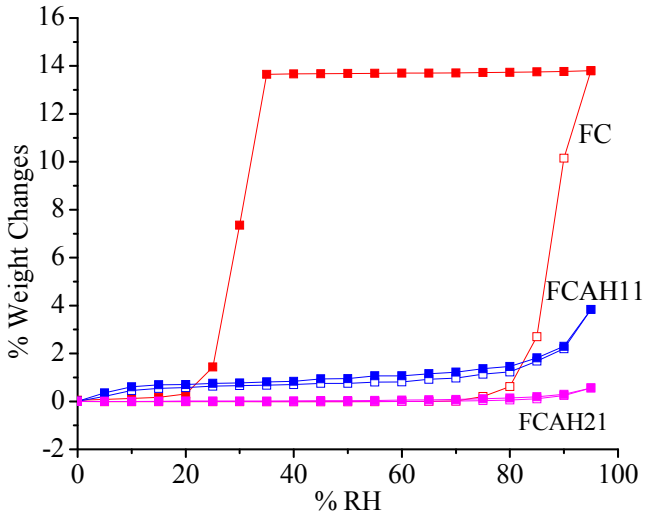

Fig. 9 DVS curves of FC, FCAH11, and FCAH21. □: moisture sorption, ■: moisture desorption.

Thermal properties

Thermodynamic property of API can be readily modified by new solid form formation. Hence, it is crucial to know and control the thermodynamic parameter of the new drug forms since the undesired melting or phase transformation has significant effect on the stability and processability. DSC curves of FCAH21, FCAH11, and the raw compounds are shown in Figure 10. The DSC curve of FC shows a sharp endothermic peak at 299 °C and followed by an intense exothermic peak which can be attributed to the melting and decomposition procedure of FC, respectively. After CAB cocrystal formation, FCAH21 exhibits only one exothermic peak at 236 °C (onset temperature 230°C, Figure 10), indicating the sample decomposition. The sample melting (endothermic peak) was not detected, which may be attributed to the concurrent of melting and decomposition. Decomposition is a kinetic process, which may shift to higher temperatures at higher heating rates. For melting, a thermodynamic process, the effect on the melt onset caused by heating rate changes is limited.[31] Thus, a DSC scan at heating rate of 50°C/min was also conducted and an endothermic event (onset temperature 236 °C, not shown here) was detected. The

decomposition/fusion temperature of FCAH21 is much higher (more than 50 °C) than room temperature (Figure 10 and Figure S5), which provides adequate thermal stability for processing and storage.

For FCAH11, a broad low temperature dehydration peak appears at ~101 °C (onset temperature ~84 °C, Figure 10) followed by decomposition/fusion of the compound at above ~120 °C (also see TG curve of FCAH11, Figure S6). FCAH11 can hold its crystal water after equilibrating at 0% RH/25 °C (*vide supra*). While, slight dehydration will occur if the temperature is elevated. From the TG curve of FCAH11 (Figure S6), such slight dehydration below 84 °C is clearly disclosed and is unsatisfactory.

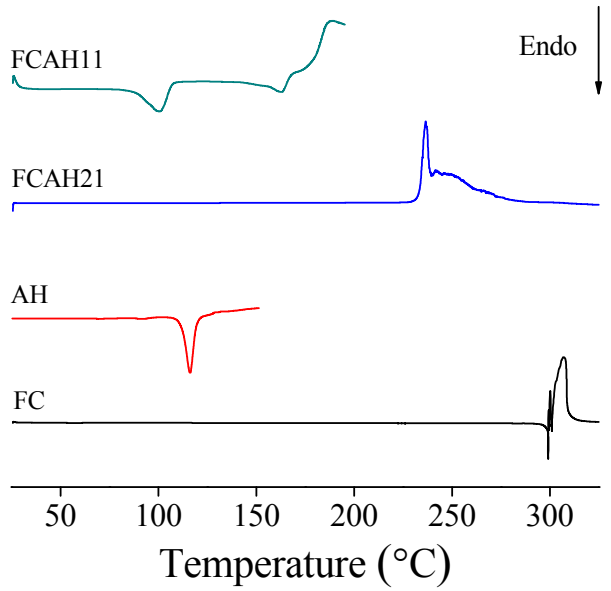

Fig. 10 DSC curves of FC, AH, FCAH21, and FCAH11.

Conclusions

A CAB cocrystal and a salt hydrate of FC in forms of FCAH21 and FCAH11 were obtained by solution crystallization and freeze-drying, respectively. Their structures were resolved by single crystal XRD measurements, and ionization states were further confirmed by solid state NMR spectra. At room temperature, both of the two sample exhibit superior phase stability against hydration over form I FC. Additionally, FCAH21 has higher API content and presents more favorable thermal stability than those of FCAH11 which highlight its potential towards further pharmaceutical applications. Further investigation on the solid-state properties, including mechanical properties and solubility of FCAH21 is currently under way.

Acknowledgements

This work was supported by the Natural Science Foundation of China (No. 21205129) and Jiangsu Provincial Fund for Natural Sciences (No. BK2012191). The NMR system used in this study was funded through the key scientific equipment plan of the Chinese Academy of Sciences (CAS). H.L.Z thanks Youth Innovation Promotion Association, CAS, for a research funding.

Notes and references

[a] Laboratory of Magnetic Resonance Spectroscopy and Imaging, Suzhou Institute of Nano-tech and nano-bionics, Chinese Academia of Sciences, Suzhou 215123, P.R. China. Tel: +86-512-62872713; Fax: +86-512-62603079; E-mail: hlzhang2008@sinano.ac.cn (HLZ), zwdeng2007@sinano.ac.cn (ZWD)

[b] Crystal Pharmatech, Suzhou Industrial Park, Suzhou 215123, P.R. China.

[c] College of Chemistry, Chemical Engineering and Materials Science, Soochow University, Suzhou 215123, P.R. China.

† Electronic Supplementary Information (ESI) available: Crystallographic Information Files (CIF), ORTEP representations, theoretical powder XRD patterns after Rietveld refinement and TG curves of FCAH21 and FCAH11. See DOI: 10.1039/b000000x/

1 S. L. Morissette, O. Almarsson, M. L. Peterson, J. F. Remenar, M. J. Read, A. V. Lemmo, S. Ellis, M. J. Cima and C. R. Gardner, *Adv. Drug Deliv. Rev.*, 2004, **56**, 275.

2 S. L. Childs, L. J. Chyall, J. T. Dunlap, V. N. Smolenskaya, B. C. Stahly and G. P. Stahly, *J. Am. Chem. Soc.*, 2004, **126**, 13335.

3 B. Rodriguez-Spong, C. P. Price, A. Jayasankar, A. J. Matzger and N. Rodriguez-Hornedo, *Adv. Drug Deliv. Rev.*, 2004, **56**, 241.

4 R. Banerjee, P. M. Bhatt, N. V. Ravindra and G. R. Desiraju, *Cryst. Growth Des.*, 2005, **5**, 2299.

5 C. Saal and A. Becker, *Eur. J. Pharm. Sci.*, 2013, **49**, 614.

6 Steed, J. W. The role of co-crystals in pharmaceutical design. *Trends. Pharmacol. Sci.* **2013**, *34*, 185–193.

7 S. L. Childs, G. P. Stahly and A. Park, *Mol. Pharmaceutics*, 2007, **4**, 323.

8 E. R. Block, A. E. Jennings and J. E. Bennett, *Antimicrob. Agents Chemother.*, 1973, **3**, 649.

9 A. Vermes, H. J. Guchelaar and J. Dankert, *J. Antimicrob. Chemother.*, 2000, **46**, 171.

10 A. T. Hulme and D. A. Tocher, *Cryst. Growth Des.*, 2006, **6**, 481.

11 (a) S. R. Perumalla, V. R. Pedireddi and C. C. Sun, *Mol. Pharmaceutics*, 2013, **10**, 2462. (b) S. R. Perumalla and C. C. Sun, *J. Pharm. Sci.*, 2014, **4**, 1126.

12 C. C. P. da Silva, R. de Oliveira, J. C. Tenorio, S. B. Honorato, A. P. Ayala and J. Ellena, *Cryst. Growth Des.*, 2013, **13**, 4315.

13 P. Prabakaran, S. Murugesan, P. T. Muthiah, G. Bocelli and L. Righi, *Acta Crystallogr.*, 2001, **E57**, o933.

14 G. Portalone, *Chem. Cent. J.*, 2011, **5**, 51(8 pages).

15 M. Tutughamiarso, G. Wagner and E. Egert, *Acta Crystallogr.*, 2012, **B68**, 431.

16 A. T. Hulme and D. A. Tocher, *Acta Crystallogr.*, 2005, **E61**, o2112.

17 G. Portalone and M. Colapietro, *J. Chem. Crystallogr.*, 2007, **37**, 141.

18 (a) S. R. Perumalla, V. R. Pedireddi and C. C. Sun, *Cryst. Growth Des.*, 2013, **13**, 429. (b) S. R. Perumalla and C. C. Sun, *Cryst. Growth Des.*, 2014, **DOI**: 10.1021/cg5005825.

19 B. R. Bhogala, S. Basavoju and A. Nangia, *CrystEngComm*, 2005, **7**, 551.

20 G. Springuel, B. Norberg, K. Robeyns, J. Wouters and T. Leyssens, *Cryst. Growth Des.*, 2012, **12**, 475.

21 F. T. Martins, N. Paparidis, A. C. Doriguetto and J. Ellena, *Cryst. Growth Des.*, 2009, **9**, 5283.
22 S. P. Velaga, V. R. Vangala, S. Basavoju and D. Bostrom, *Chem. Commun.*, 2010, **46**, 3562.
23 *APEX2* User Manual, Version 1.2.7; Bruker AXS Inc.: Madison,WI, 2005.
24 (a) G. M. Sheldrick, *Acta Crystallogr*., 2008, **A64**, 112. (b) G. M. Sheldrick, *SHELXS-97*, Program for Structure Solution; University of Göttingen: Göttingen, Germany, **1999**. (c) G. M. Sheldrick, *SHELXL-97*, Program for Structure Refinement, University of Göttingen: Göttingen, Germany, **1997**.
25 M. D. Eddleston, B. Patel, G. M. Day and W. Jones, *Cryst. Growth Des.*, 2013, **13**, 4599.
26 F. G. Vogt, J. S. Clawson, M. Strohmeier, A. J. Edwards, T. N. Pham and S. A. Watson, *Cryst. Growth Des.*, 2009, **9**, 921.
27 A. Burgard, U.S. patents US2002/0197381A1 and US2005/6849623B2.
28 S. Aitipamula, V. R. Vangala, P. S. Chow and R. B. H. Tan, *Cryst. Growth Des.*, 2012, **12**, 5858.
29 S. Basavoju, D. Boström and S. P. Velaga, *Mol. Cryst. Liq. Cryst.*, 2012, **562**, 254.
30 S. R. Perumalla and C. C. Sun, *CrystEngComm*, 2013, **15**, 5756.
31 M. J. Bevill, P. I. Vlahova and J. P. Smit. *Cryst. Growth Des.*, 2014, **14**, 1438.